Influence of sand supply and grain size on upper regime bedforms

Sydney Sanders[1], Sadegh Jafarinik[1,2], Ricardo Hernandez Moreira[1,3], Ryan Johnson[1], Amanda Balkus[1], Mahsa Ahmadpoor[1], Brandon Fryson[1], Briana McQueen[1], Juan Fedele[4] and Enrica Viparelli[1]

[1]Department of Civil and Environmental Engineering, University of South Carolina, Columbia, USA
[2]Arcadis U.S., Inc., Columbus, Ohio, USA
[3]Hanson-Rodríguez SRL, Santo Domingo, Dominican Republic
[4]Exxon Mobil Upstream Research Company, Houston, Texas, USA

Corresponding author Enrica Viparelli (viparell@cec.sc.edu)

Key points

- The ratio of volume transport of sediment to volume transport of water Q_s/Q_w plays a prime control on equilibrium bed configuration
- The wavelength of upstream migrating bedforms increases with the ratio between sediment supply and flow discharge
- The presence of suspended bed material load seems to favor the formation of upstream migrating bedforms

Abstract

Notwithstanding the large number of studies on bedforms such as dunes and antidunes, performing quantitative predictions of bedform type and geometry remains an open problem. Here we present the results of laboratory experiments specifically designed to study how sediment supply and caliber may impact equilibrium bedform type and geometry in the upper regime. Experiments were performed in a sediment feed flume with flow rates varying between 5 l/s and 30 l/s, sand supply rates varying between 0.6 kg/min and 20 kg/min, uniform and non-uniform sediment grain sizes with geometric mean diameter varying between 0.22 mm and 0.87 mm. The experimental data and the comparison with datasets available in the literature revealed that the ratio of the volume transport of sediment to the volume transport of water Q_s/Q_w plays a prime control on the equilibrium bed configuration. The equilibrium bed configuration transitions from washed out dunes (lower regime), to downstream migrating antidunes (upper regime) for Q_s/Q_w between 0.0003 and 0.0007. For values of Q_s/Q_w greater than those typical of downstream migrating antidunes, the bedform wavelength increases with Q_s/Q_w. At these high values of Q_s/Q_w equilibrium bed configurations with fine sand are characterized by upstream migrating antidunes or cyclic steps, and significant suspended load. In experiments with coarse sand, equilibrium is characterized by plane bed with bedload transport in sheet flow mode. Standing waves form at the transition between downstream migrating antidunes and bed configurations with upstream migrating bedforms.

Plain Language Summary

Bedforms are bumps made of sediment that form and move in channels transporting water and sediment. Their size and direction of movement depend on the properties of the flow and of the sediment. Although bedforms have been observed and studied for long time, predicting their type and size remains an open problem. Here we present results of laboratory experiments designed to study bedforms made of sand that form in presence of fast flows. Our results show that, in these conditions, bedform type and size depend on the ratio between volumes of transported sediment and water. In addition, our results suggest that if sand is transported in a thin layer near the bed, bedforms tend to move in the direction of the flow, while bedforms tend to move in the direction opposite to the flow if some sand is suspended in the water.

1. Introduction

The interaction between the flowing water and a mobile bed composed of loose sediment often results in the formation of bedforms in both shallow (fluvial, coastal and glacigenic) and deep-water settings (Parkash and Middleton, 1970, Paola et al., 1989, Alexander et al., 2001, Araya and Masuda, 2001, Best, 2005, Spinewine et al., 2009, Kostachuk et al., 2009, Covault et al., 2017, Froude et al., 2017, Lang et al., 2021). In general, bedforms can be divided in two broad categories, bedforms with height and wavelength that are strongly dependent on the flow depth and bedforms with geometry that is primarily dependent on channel width, or on the ratio between channel width and depth (Hayashi and Ozaki, 1979, Ikeda, 1984, Garcia, 2008). In this paper we present experimental results on bedforms with geometry dependent on channel depth, such as dunes and antidunes. The scope of the experiments was to understand if and how antidune geometry and migration direction varied with sand supply rate, grain size and preferential mode of transport, these being bedload or suspended load.

Bedforms have been studied in the field and with laboratory experiments to determine the influence on flow resistance and sediment transport (Einstein and Barbarossa, 1952, Simons and Richardson, 1962, 1966, Engelund and Hansen, 1967, Brownlie, 1981, Fedele, 2003, Wright and Parker, 2004a, b, Sequeiros et al., 2010, Yokokawa et al., 2010, Fedele et al., 2016, Myrow et al., 2018, Latosinski et al., 2022). Bedforms and the associated sediment sorting are also studied to interpret stratifications in the rock record, understand channel morphology, reconstruct flow properties, predict the permeability of the subsurface and the accumulation of sediments with certain characteristics such as heavy minerals (Bourgeois, 1980, Best and Brayshaw, 1985, Slingerland and Smith, 1986, Hughes Clarke et al., 1990, Carling et al., 2000a, b, Endo et al., 2002, Blom et al. 2003, Kleinhans, 2005, Jerolmack and Mohrig, 2005, Garcia, 2008, Naruse et al., 2012, Hiscott et al., 2013, Carling, 2013, Postma et al., 2014, Cartigny et al., 2011, 2014, Viparelli et al., 2015, Carling and Leclair, 2019).

As a result of these studies, bedform progression is well understood for fine sands, defined here as sands with characteristic grain size smaller than 0.5 mm (Garcia, 2008). If we consider a laboratory flume with a plane bed covered with uniform, fine sand and we imagine a gradual increase of the flow velocity, we first observe water flowing on an immobile bed, then sediment grains start moving and ripples form. As the flow velocity further increases, bedforms evolve into dunes, which migrate downstream. In the presence of dunes, the water and the bed surface are in opposition of phase, that is the water surface is low on the dune crests and it is high on the dune troughs. At relatively high velocities dunes are washed out and the bed becomes flat again. At even higher flow velocities, antidunes form and migrate in the upstream direction. In presence of antidunes the water surface is in phase with the bed. Another increase in flow velocity results

in the formation of cyclic steps, upstream migrating bedforms with hydraulic jumps forming between consecutive steps (Simons and Richardson, 1962, Engelund and Hansen, 1967, Taki and Parker, 2005).

In the presence of coarse sand ripples do not form (Simons and Richardson, 1966). At relatively small velocities, sediment is transported on a flat bed and dunes form as the flow velocity increases (Engelund and Hansen, 1967). This flat bed configuration is referred to as *lower regime plane bed*. The flat bed configuration at the transition between dunes and antidunes is called *upper regime plane bed* and sediment transport is characterized by individual grains rolling "almost continuously downstream in sheets one or two grain diameters thick" (Simons and Richardson, 1966). In presence of coarse sand and shallow flow the upper regime plane bed may not form and, as the flow velocity increases, the bed configuration transitions from dunes to antidunes (Simons and Richardson, 1966).

Hernandez Moreira (2016) and Hernandez Moreira et al. (2020) noticed that in experiments with ~1 mm sand the bed became flat at flow velocities higher than those typical of the antidune regime. In this bed configuration sand was transported in a near bed layer of colliding grains with thickness of ten grain diameters or more. This near bed layer is called *sheet flow layer* (Wilson, 1987).

The upper regime plane bed with bedload transport in sheet flow mode can be characterized by the presence of long wavelength and small height bedforms that could only be identified in pictures taken far away from the flume windows and in time series of bed elevations (Hernandez Moreira et al., 2020). These long wavelength bedforms are different from those at the dune-antidune transition observed by Paola et al. (1989) and Bridge and Best (1988). The Hernandez Moreira et al. (2020) bedforms were obtained with values of the Froude number higher than 1.4 and resulted in the emplacement of structureless (massive) deposits. The bedforms described by Paola et al. (1989) and Bridge and Best (1988) were obtained with values of the Froude number smaller than 1.2, in absence of sheet flow and resulted in the emplacement of parallel laminated deposits (Best and Bridge, 1992).

Laboratory experiments and analytical work clearly showed that antidunes can also migrate in the downstream direction (Kennedy, 1961, Fukuoka et al., 1982, Engelund and Fredsoe, 1982, Nunez-Gonzalez and Martin-Vide, 2010, Yokokawa et al., 2010, Hernandez Moreira, 2016, Hernandez Moreira et al., 2020). The analytical work by Engelund (1970) and Fredsoe (1974), the Yokokawa et al. (2011) phase diagram and the experiments by Spinewine et al. (2009) and Yokokawa et al. (2011) suggest that the presence of bedload transport may be important for the formation of downstream migrating antidunes. Carling and Shvidchenko (2002), however, reported the formation of upstream migrating antidunes in gravels with characteristic grain size smaller than 7 mm at relatively high Froude numbers. Unfortunately, these authors do not discuss the mode of bed material transport.

Downstream migrating antidunes maintain the geometry as they travel downstream (Hernandez Moreira, 2016). Depending on the properties of the flow and of the sediment, upstream migrating antidunes either migrate upstream at relatively small velocities and maintain their shape, or rapidly move upstream, grow until they become unstable, break and the bed becomes plane until a new train of upstream migrating antidunes forms (breaking antidunes) (Simons and Richardson, 1966, Yokokawa et al., 2011).

All these studies notwithstanding, the development of reliable predictors of equilibrium bedform type and geometry remain an open problem (Garcia, 2008). Phase diagrams based on empirical data or mathematical modeling were proposed to determine the equilibrium bed configuration in terms of non-dimensional parameters representative of the flow conditions and of the sediment properties (see e.g., Simons and Richardson, 1966, Engelund, 1970, Vanoni, 1974, Southard and Boguchwal, 1990, Garcia, 2008, Yokokawa et al., 2011, Ohata et al., 2018, Pen et al., 2018). Relations to predict the equilibrium bedform geometry as a function of the properties of the flow and of the sediment were primarily proposed for ripples and dunes but developing reliable predictors of bedform height and wavelength remains a challenge (Engelund and Fredsoe, 1982, van Rijn, 1984, Garcia, 2008).

Here we focus on how equilibrium antidune geometry varies with sediment supply and caliber. We performed laboratory experiments specifically designed to determine if the ratio of the volume transport of sediment to the volume transport of water, as well as the mode of bed material transport (bedload or suspended load), play a role on upper regime bedform type and shape.

This paper is organized as follows, we present an overview of the experimental program followed by the description of the experimental set up and procedures. Experimental results are then presented and analyzed to identify how bedform wavelength, flow depth and the presence of suspended bed material load varies with sediment grain size and with the ratio between the volume of transported sand and the flow discharge. Finally, our results are compared with previous on open channel flow experiments.

2. Overview of the experiments

Laboratory experiments were conducted in a sediment feed flume with glass walls at the Hydraulics Laboratory at the Department of Civil and Environmental Engineering, University of South Carolina. The flume is 13 m long, 0.5 m wide and 0.9 m deep. A sediment trap is placed 9 m downstream of the flume entrance and a tailgate controls the downstream water surface level. A calibrated orifice plate and a Dwyer series 490 wet-wet manometer were used to measure the flow rate from the head tank.

To decrease the sediment supply needed during the experiments and the occurrence of three-dimensional bedforms, the cross-section of the test reach was narrowed to 0.19 m with the use of marine plywood. A schematic view of the flume is presented in Figure 1. In the first 2 m of the flume the cross section was

gradually narrowed with marine plywood to 0.19 m to obtain a 7 m long experimental test reach (Jafarinik et. al, 2019; Hernandez Moreira et. al, 2020). The sand transported in suspension was deposited downstream of the sediment trap. As further discussed below, a siphon rake was used to measure suspended sediment concentration profiles.

Experiments were designed based on previous work performed in the same flume with uniform sand with geometric mean size D_g equal to 1.1 mm, and with non-uniform sand with D_g equal to 0.95 mm. In these experiments, flow rates were equal to 30 l/s and 20 l/s and sediment feed rates varied between 0.5 kg/min and 20 kg/min. For feed rates smaller than 3 kg/min, washed-out dunes formed. Downstream migrating antidunes formed for feed rates between 3 kg/min and 12 kg/min, and plane bed with bedload transport in sheet flow mode was obtained for feed rates equal to 16 kg/min and 20 kg/min (Hernandez Moreira, 2016, Hernandez Moreira et al., 2020).

Experiments presented herein are summarized in Table 1 in terms of geometric mean diameter of the sediment D_g, flow rate Q_w, and mass feed rate G_s. Experiments are named with a number and the name initials of the lead experimentalist, for example, 1-SS denotes the first experiment ran by Sydney Sanders and 9-SJ denotes the ninth experiment ran by Sadegh Jafarinik. The sediment used in experimental runs 1-SJ – 4 SJ was the non-uniform sand used in the Jafarinik et al. (2019) experiments, with D_g = 0.87 mm and grain size distribution similar to the sand used by Hernandez Moreira et al. (2020). These experiments were performed to investigate the role of the water depth (flow rate) on the formation of upper regime bedforms. In particular, the flow rate was equal to 15 l/s and 8 l/s, smaller than in the Hernandez Moreira (2016) and Hernandez Moreira et al. (2020) experiments.

Experiments 5-SJ to 9-SJ and 1-SS to 7-SS were designed to study the role of the mode of sand transport on upper regime bedforms. The flow rates varied between 5 l/ and 30 l/s and the feed rates varied between 0.6 kg/min and 20 kg/min, which are in the same range of our previous experiments. Two uniform quartz sands with D_g equal to 0.22 mm and 0.62 mm were used in experiments 5-SJ to 9-SJ and 7-SS. These uniform sands were mixed to obtain the sediment used in the other SS experiments.

Experiments 1-SS to 3-SS were performed with non-uniform sand with D_g equal to 0.43 mm and geometric standard deviation σ_g equal to 1.85 mm. In experiments 4-SS to 6-SS, the grain size distribution of experiment 3-SS was made finer by adding one scoop of 0.22 mm sand for every one scoop of sediment mixture, resulting in a new mixture with D_g equal to 0.34 mm and σ_g equal to1.95 mm. The grain size distributions of the sediment used in the experiments and collected downstream of the sediment trap in the SS experiments are presented in Figure 2, where legend labels correspond to the sand D_g. The grain size of the sediment collected downstream of the sediment trap in the SS experiments is considered to be representative of the sediment transported in suspension.

3. Experimental procedure

The experiments started from a disequilibrium (net-depositional or net-erosional) condition and continued until the flow and the sediment transport reached equilibrium, that is when the bed and the water surface elevation averaged over a series of bedforms did not change in time. At equilibrium, suspended sediment concentration was measured, and the experiment terminated.

Experiment 1-SJ started with a nearly empty flume, that is few bags of sand were emptied to cover the bottom of the flume and favor initial sediment deposition in the test reach. The initial water depth was equal to ~25 cm. At equilibrium the elevation of the alluvial deposit above the bottom of the flume was on the order of 10-20 cm. Experiments 2-SJ to 4-SJ started using the equilibrium deposit from the previous experiments. For example, the initial bed of experiment 3-SJ was the equilibrium bed obtained at the end of experiment 2-SJ. Prior to experiment 5-SJ the flume was emptied because we changed the sediment grain size. In particular, the non-uniform sand of experiments 1-SJ to 4-SJ was substituted with a uniform sand with D_g = 0.62 mm. Experiment 8-SJ, which was performed with the finest sand, also started with a nearly empty flume, as experiments 1-SJ and 5-SJ.

Experiment 1-SS started with a 10 cm thick layer of sand with D_g equal to 0.43 mm. Water discharge and sediment feed rate were turned on at the specified rates and the experiment was run until equilibrium. In the following runs, the equilibrium bed of the previous experiment was used as initial condition for the next experimental run. For example, the initial deposit in experiments 2-SS, was the equilibrium bed of experiments 1-SS. After experiment 3-SS, an approximately 3 cm thick layer of sand with D_g equal to 0.34 mm was sprinkled over the existing deposit to perform experiments with a finer sediment grain size. This process was repeated once more before experiment 7-SS by sprinkling instead coarse sediment with D_g equal to 0.62 mm. The duration of each experiment varied between 45 minutes to two hours, depending on time required to reach equilibrium.

3.1 Measurements of bed and water surface profiles

Vertical and horizontal rulers on the glass wall and at the top of the flume indicated the distance from the flume entrance and the elevation above the flume bed. Bed and water surface elevations were measured with ruler readings at intervals moving downstream of 10 cm in the SJ experiments and of 20 cm in the SS experiments (Hernandez Moreira et al., 2020). The first measurement was recorded at 2.2 m from the flume entrance in the SJ experiments and at 3.50 m in the SS experiments. The last measurement was taken approximately at 8.85 m from the flume entrance.

During the experiments, measured values were reported in a spreadsheet, plotted and the slopes of the best fit lines were computed to estimate the bed slope and the water surface slope. When the bed and water

surface slopes did not significantly change in time, the flow and the sediment transport were deemed to be at equilibrium (Viparelli et al., 2015, Hernandez Moreira et al., 2020). Equilibrium profiles were then used to compute relevant flow parameters.

Equilibrium water depth and slopes were respectively determined as the average water depth (difference between the measured water surface and the bed elevation) and bed slope of the last measured longitudinal profile determined with a linear regression.

Experiments were performed in a 0.19 m wide laboratory flume with water depths varying between 0.04 m and 0.13 m. The width to depth ratio was thus smaller than 5 and the cross section was considered narrow. In a narrow cross section, the difference in roughness between the sediment covered bed and the smooth side walls must be accounted for to estimate the bed shear stress acting on the bed (Vanoni and Brooks, 1957).

We followed the procedure introduced by Vanoni and Brooks (1957) as formulated by Chiew & Parker (1994), and we refer to Jafarinik et al. (2019) and Hernandez Moreira et al. (2020) for details on the implementation. For the calculation of the sidewall corrected bed shear stress and friction coefficient the cross section was divided into two, non-interacting regions, the bed region and the wall region. It was further assumed that 1) the Darcy-Weisbach resistance relationship held for the entire cross section and for both the bed and wall regions, 2) the downstream pull of gravity was balanced by the shear stress acting on the walls and, on the bed, and 3) the mean flow velocity and the energy gradient were the same for the cross section, the bed, and the wall regions. Under these assumptions, the conservation of mass and momentum were imposed and the Nikuradse equation for smooth pipes was used to compute the flow resistance in the wall region.

In presence of bedforms, flow resistance is related to the presence of a granular bed (skin friction) and may be affected by the interaction between the flow and the bedforms (form drag). Stresses that act tangentially to the bed, known as skin friction, are critical to sediment entrainment and bedload transport. When no bedforms are present, the drag on the bed is only associated with skin friction (Einstein and Barbarossa, 1952, Parker, 2004).

For the partition of the flow resistance between skin friction and form drag, an ideal flat bed configuration was considered. This ideal flow had the same grain roughness, energy slope and mean flow velocity as there was presence of bedforms. The hydraulic radius and the bed friction coefficient associated with skin friction were computed with the use of the 1) Manning-Strickler relation, and 2) the product of the hydraulic radius and the energy slope to compute the bed shear stress associated with skin friction. We refer to Jafarinik et al. (2019) and Hernandez Moreira et al. (2020) for details on the calculation procedure.

3.2 Measurements of suspended sediment concentration

The volumetric suspended sediment concentration, c, was measured with a rack of six siphons located approximately 2 cm apart. The samples were collected into 1500 cm^3 containers, the suspension was then filtered, the sediment was dried, weighted and the volumetric concentration was computed. To convert sediment weight into volumes, a density equal to 2.65 gr/cm^3 was used.

Measurements of suspended sediment concentration were performed in experimental runs 1-SS to 6B-SS, 5-SJ to 7SJ, 9-SJ and 10-SJ. In the SJ experiments, the rack was placed at 8.2 m from the flume entrance and the distance between the siphon closest to the deposit and the deposit was kept equal to few percent of the flow depth. In the SS experiments, the rack was placed close to the downstream end of the bed deposit. The distance between the siphon closest to the deposit and the deposit varied from one experiment to the other because the rack was anchored to the flume sidewalls.

4. Results

Experimental results are summarized in Table 2 in terms of equilibrium bed slope S, equilibrium flow depth H, Froude number associated with skin friction Fr_o, equilibrium bedform height and wavelength Δ and λ, bedform migration rate v and bed configuration. Bedform height, wavelength and migration rate were measured using rulers attached to the flume and from the analysis of video recordings.

The resulting equilibrium bed configuration was classified by using observations during the experiments of the bed and water surface. If the bed and the water surface were in opposition of phase, bedforms were classified as washed-out dunes WD because of the relatively high (but still subcritical) Froude numbers. If the bed and the water surface were in phase, migrating bedforms were classified as antidunes and non-migrating bedforms were considered standing waves SW. Depending on the migration direction, antidunes were classified as upstream UA or downstream migrating DA. The plane bed configurations were classified based on the mode of bedload transport either in upper plane bed with a few grain diameters thick bedload layer UP or upper regime plane bed with bedload transport in sheet flow mode PS.

In experiments 5-SS and 7-SS, the shape of the upstream migrating antidunes and of the associated water surface wave did not change dramatically in time as they migrated upstream (Figures 3a and 3b and supplementary video 1). In experiment 4-SS, the deformation of the bed and water surface was larger than in experiments 5-SS and 7-SS and the amplitude of the water surface wave became so large that the wave broke, and the bed locally flattened (Figure 3c, and supplementary video 2). In experiments 3-SS, 6A-SS and 6B-SS the deformation of the water surface became so strong that the waves regularly broke, the bed became flat until a new train of upstream migrating antidunes formed. These bedforms are called breaking

antidunes (Simons et al., 1966), and are shown in Figures 3d (experiment 3-SS), 3e and 3f (experiment 6B-SS) and in the supplementary videos 3 and 4.

The Engelund phase diagram after Parker (2004) (see also Figure 2-37 in Garcia, 2008) is utilized to compare our experiments with a classification of the bed configurations based on mathematical modeling and other experimental observations (Figure 4). In the phase diagram, lower regime bedforms and upper regime bedforms are identified based on Fr_o and the non-dimensional wavenumber k defined as $2\pi H_o/\lambda$, where H_o is the flow depth associated with skin friction. The black lines in Figure 4 identify three regions of the (k, Fr_o) plane corresponding to lower regime and upper regime with bedform migrating upstream or downstream. Black marker lines indicate experiments of Table 2, grey marker lines identify experiments by Hernandez Moreira (2016) and Hernandez Moreira et al. (2020). Symbols with no fill indicate experiments with coarse sand ($D_g > 0.5$ mm) and grey filled symbols are experiments with fine sand ($D_g \leq 0.5$ mm). Circles represent washed-out dunes, diamonds upper plane bed with a few grain diameters thick bedload layer, triangles downstream migrating antidunes and squares upstream migrating antidunes. The 'x' represents standing waves and fine sand (experiment 2-SS). The '+' are coarse sand experiments with upper plane bed and bedload transport in sheet flow mode.

Most of the data pertaining to the experiments with fine sand are in the region of upstream migrating bedforms, while data from upper regime experiments with coarse sand are either in the region of downstream migrating bedforms or close to the boundary between the upstream and downstream migrating bedforms (Figure 4). This suggests that sediment size and the mode of sediment transport may play a significant role on the migration direction of upper regime bedforms and on the bed configurations, as analytically observed by Ohata et al. (2021).

This observation is reinforced in Figure 5, where measurements of suspended sediment concentration are presented with the non-dimensional elevation above the channel bed z/H on the vertical axis and the volumetric suspended sediment concentration c on the horizontal axis. Here z denotes an upward oriented vertical coordinate with origin on the channel bed and H is the water depth. Line colors indicate the geometric mean size of the sand used in the experiments and symbol colors refer to the bed configuration. Grey, red, blue and black lines represent experiments with sand D_g equal to 0.62 mm, 0.43 mm, 0.34 mm and 0.22 mm, respectively. Green, black, red, blue and yellow symbols respectively denote bed configurations of washed out dunes, downstream migrating antidunes, plane bed, standing waves and upstream migrating antidunes. The red-yellow symbol indicates a bed configuration at the transition between standing waves and upstream migrating antidunes (experiment 10-SJ).

In the experiments with upstream migrating antidunes the volumetric suspended sediment concentration is about one order of magnitude higher than in the experiments with other bed configurations, suggesting that

the presence of suspended bed material load may play a prime control on bedform migration direction (see also Engelund, 1970 and Fredsoe, 1974). Measurements of Figure 5 and the grain size distributions of the sediment transported in suspension of Figure 2 show that at the relatively high flow velocities typical of the antidune regime, sand can be either transported as bedload or as suspended load. In the experiments presented herein, sand with grain size smaller than 0.3 mm was preferentially transported in suspension and sand with grain size coarser than 0.3 mm was preferentially transported as bedload. It is important to note that the fine sand did not behave as wash load because it was found in significant quantities in the bed deposit.

4.1 Equilibrium bedform geometry and migration direction

In the experiments of Table 1 and Table 2, different equilibrium bed configurations were obtained by changing the flow discharge, the sediment feed rate and the sediment size distribution. A close look to Table 2 shows that equilibrium bed configuration and bedform geometry change as the flow discharge (and thus the water depth), the sediment feed rate and grain size vary.

In response to an increase in sediment feed rate, the equilibrium bedform wavelength increases. In Figure 6 pictures taken during experiments 4-SS, 5-SS and 6A-SS with fine sand (D_g = 0.34 mm) clearly show that when the mass feed rate G_s increased from 10 kg/min to 15 kg/min to 20 kg/min and the flow rate Q_w was kept equal to 10 l/s, antidune wavelength increased from 50 cm to 80 cm.

Similar behavior was observed in experiments with coarse sand. Runs 2-SJ and 3-SJ were performed with sediment with D_g equals to 0.87 mm and flow discharge Q_w equals to 15 l/s. In these runs, the wavelength increased from 30 cm to 45 cm as the feed rate increased from 6 kg/min to 16 kg/min. The sediment used in runs 6-SJ and 7-SJ had D_g equal to 0.62 mm, the flow discharge was 15 l/s and, as the feed rate increased from 2.2 kg/min to 6.9 kg/min, the wavelength increased from 25 cm to 35 cm, as shown in Figure 7. Hernandez Moreira (2016) and Hernandez Moreira et al. (2020), noticed a similar behavior in upper regime experiments with coarse sand. As the sediment feed rate increased, equilibrium downstream migrating upper regime bedforms became longer.

The response of the equilibrium bedform height to an increase in sediment feed rate depended on sediment grain size. In runs with fine sand of Figure 6, the equilibrium height of the upstream migrating antidunes increased with the sediment supply. In the runs performed with coarse sand, the equilibrium height of the downstream migrating antidunes decreased in response to an increase in sediment transport rate (Figure 7). In particular, in the experiments with D_g = 0.87 mm downstream migrating antidunes (2-SJ) evolved into an upper plane bed with bedload transport in sheet flow mode (3-SJ). In experiments with D_g = 0.62 mm downstream migrating antidunes (6-SJ) evolved into upper regime plane bed with standard mode of bedload

transport (7-SJ). These results agree with previous experiments with D_g approximately equal to 1 mm. In response to an increase in sediment supply, bedform height decreased as the equilibrium bed configuration transitioned from downstream migrating antidunes to plane bed with bedload transport in sheet flow mode (Hernandez Moreira, 2016 and Hernandez Moreira et al., 2020).

The response of the equilibrium bed configuration to the increase in sediment supply in experiments 1-SJ to 3-SJ with sand D_g = 0.87 mm resulted in a transition from washed-out dunes to downstream migrating antidunes and plane bed with bedload transport in sheet flow mode, as also observed during the Hernandez Moreira (2016) and Hernandez Moreira et. al (2020) experiments. In experiments 5-SJ to 7-SJ with sand D_g = 0.62 mm and discharge of 15 l/s, as the feed rate increased from 1 kg/min to 6.9 kg/min the equilibrium bed configuration varied from washed out dunes to downstream migrating antidunes to upper plane bed with a few grain diameters thick bedload layer. A further increase in sediment feed rate from 6.9 kg/min to 10 kg/min associated with a decrease in flow discharge from 15 l/s to 10 l/s, resulted in a change in bed configuration from the plane bed of experiment 7-SJ to the upstream migrating antidunes of experiment 7-SS.

In experiments 1-SS, 2-SS and 3-SS the flow discharge decreased from 30 l/s to 20 l/s to 10 l/s, the sediment feed rate was equal to 10 kg/min and the sand had D_g equal to 0.43 mm. In response to this reduction in flow discharge, the equilibrium flow depth decreased, the equilibrium slope increased, and we observed the following change in equilibrium bed configuration: upper plane bed in experiment 1-SS, standing waves in experiment 2-SS, and upstream migrating antidunes in experiment 3-SS (Figure 8).

Another change in bed configuration associated with a change in flow discharge, and thus equilibrium water depth and slope, was observed in experiments 2-SJ and 4-SJ. As the flow discharge decreased from 15 l/s in experiment 2-SJ to 8 l/s in experiment 4-SJ, the water depth decreased from 6.18 cm to 3.97 cm and the bed slope increased from 1.1% to 1.8%. In response to this change in equilibrium flow conditions, the bed configuration changed from downstream migrating antidunes to upper plane bed (Figure 8).

A change in flow discharge Q_w, and thus equilibrium water depth and bed slope, is not necessarily associated with a change in equilibrium bed configuration. In experiments 6A-SS and 6B-SS, as Q_w decreased from 10 l/s to 5 l/s, the breaking antidune height decreased from 5.5 cm to 3 cm and the wavelength increased from 90 cm to 100 cm.

Similarly, if we compare experiments 1-SJ, 2-SJ and 3-SJ with the experiments by Hernandez Moreira (2016) with the same sediment feed rate and similar sediment sizes, we note that a change in flow discharge from 30 l/s to 15 l/s did not result in a change in bed configuration. However, bedform height and wavelength in the experiments with Q_w equal to 15 l/s were smaller than in the experiments with Q_w equal

to 20 l/s and 30 l/s, as shown in Table 3 where the Hernandez Moreira experiments are denoted as RHM. Interestingly, a change in flow discharge from 30 l/s to 20 l/s did not result in a significant change in washed out dune height, but it caused a dramatic height reduction of the long wavelength bedforms observed in the upper plane bed with bedload transport in sheet flow mode. This suggests that a threshold water depth H_{lim} may exist for each bed configurations such that a change in water depth does not result in a change in equilibrium bedform geometry if $H > H_{lim}$. However, when $H < H_{lim}$ a change in water depth results in a change in equilibrium bedform geometry or bed configuration.

A change in antidune migration direction associated with a change in sediment grain size and water discharge was observed in experiments 6-SJ and 10-SJ. In these runs the feed rate was equal to 2.2 kg/min, water discharge decreased from 15 l/s (6-SJ) to 8 l/s (10-SJ) and the sediment geometric mean size decreased from 0.62 mm (6-SJ) to 0.22 mm (10-SJ). Antidunes migrated in the downstream direction in run 6-SJ. Bedforms in run 10-SJ were close to the standing wave-antidune transition and slowly migrated upstream.

The effect of sediment size on upstream migrating antidunes was also observed by comparing experiments 3-SS, 4-SS and 7-SS. The flow discharge was 10 l/s, the feed rate was 10 kg/min, and the sand geometric mean size was 0.43 mm, 0.34 mm and 0.62 mm in experiments 3-SS, 4-SS and 7-SS, respectively. The comparison between antidune geometry revealed that the wavelength did not change with sediment size, but antidune height was highest and the migration rate was fastest in run 4-SS, that is with the finest sediment size.

5 Non-dimensional summary of the results and comparison with other datasets

The results of the experiments presented above, in Hernandez Moreira (2016) and Hernandez Moreira et al. (2020) are summarized in Figure 9 in terms of 1) ratio Q_s/Q_w between the volumetric sand (bed material) load and the flow discharge, 2) sediment size, that is fine sand ($D_g \leq 0.5$ mm) or coarse sand ($D_g > 0.5$ mm) sand, 3) bed configuration, 4) non-dimensional bedform wavelength λ/H and λ/D_g respectively in panels a and b, 5) non-dimensional bedform height Δ/H in panel c, and 6) ratio between the shear velocity u^* and the settling velocity of the sand geometric mean size v_s in panel d.

Equilibrium bed configurations in Figure 9 are washed out dunes (WD), upper plane bed with a few grain diameters thick bedload layer (UP), downstream migrating antidunes (DA), standing waves (SW), upper regime plane bed with bedload transport in sheet flow mode (PS) and upstream migrating antidunes (UA). In agreement with what observed in fine sand (Engelund and Hansen, 1967) as Q_s/Q_w increases, the equilibrium bed configuration transitions from lower to upper regime (Simons and Richardson, 1962). Our data suggest that this transition occurs for values of Q_s/Q_w between 0.0003 and 0.0007.

In addition, a second transition between equilibrium bed configurations seems to characterize the upper regime. For values of Q_s/Q_w smaller than 0.0015 antidunes migrated downstream. When Q_s/Q_w was larger than 0.0032 two equilibrium bed configurations formed depending on the sand size. Upstream migrating antidunes formed in experiments with fine sand, while upper plane bed with bedload transport in sheet flow mode characterized the equilibrium bed in experiments with coarse sand. The sand used in run 7-SS had D_g = 0.62 mm and downstream migrating antidunes formed suggesting that the boundary between coarse and fine sand used in this paper D_g = 0.5 mm should be refined. Upper plane bed with a few grain diameters thick bedload layer and standing waves occurred for values of Q_s/Q_w between 0.0015 and 0.0032.

As Q_s/Q_w increased and the equilibrium bed configuration transitioned from washed out dune to upper regime, the parameter λ/H remained relatively unchanged with bedform wavelength equal, on average, to 3-4 times the water depth (Figure 9a). On the contrary, the parameter λ/D decreased as Q_s/Q_w increased, indicating that bedforms shortened across the washed out dune – upper regime transition (Figure 9b). Further increasing Q_s/Q_w, the equilibrium bedform wavelength increased across the transition between downstream migrating antidunes and bed configurations with upstream migrating bedforms or sheet flow. This change in wavelength suggests that equilibrium bed configurations in fine sand at values of Q_s/Q_w higher than those discussed herein might be characterized by very long, upstream migrating bedforms such as chutes and pools and cyclic steps (Figure 9, panels a and b).

Non-dimensional bedform height Δ/H increased with Q_s/Q_w from the washed out dune configuration to the limit between downstream migrating antidunes and other upper regime bedforms. In particular, Δ was approximately equal to 20% of the flow depth in the washed out dune experiments and increased up to 50% of H in the experiments with downstream migrating antidunes. For values of Q_s/Q_w greater than 0.0032, the non-dimensional equilibrium bedform height Δ/H increased in the experiments with fine sand and decreased in the experiments with coarse sand (see also Figures 6 and 7). In particular, at high values of Q_s/Q_w the equilibrium bed configuration is characterized by upstream migrating bedforms in fine sand and by upper plane beds with bedload transport in sheet flow mode in coarse sand.

The ratio u^*/v_s on the vertical axis of Figure 9d indicates if sand is preferentially transported as bedload, $u^*/v_s < 1$, or if there is significant suspended sand load, $u^*/v_s > 1$ (Garcia, 2008). In the majority of the experiments, sand was preferentially transported as bedload for values of Q_s/Q_w smaller than 0.0032. However, two washed out dune experiments with fine sand and significant suspension suggest that the presence of suspended bed material load does not necessarily control the type of equilibrium bed configuration at the transition between the lower and upper regime, that is for $Q_s/Q_w < 0.0007$. Sand was preferentially transported as bedload in the experiments with equilibrium downstream migrating antidunes and plane bed, while significant suspended sand load characterized the experiments with upstream migrating antidunes (Figure 5, Hernandez Moreira, 2016, Hernandez Moreira et al., 2020). In summary,

Figure 9d suggests that significant suspended bed material load is important for the development of equilibrium bed configurations with upstream migrating bedforms, in agreement with analytical work by Engelund (1970) and Fredsoe (1974).

To determine if the classification of lower and upper regime bedforms, and of upper regime bedforms migrating downstream, upstream or in presence of bedload transport in sheet flow mode, proposed in Figure 9, can be extended to other conditions, we plotted the data by Kennedy (1961), Guy et al. (1966) and Fukuoka et al. (1982) in the non-dimensional plots of Figure 9. The comparison is presented in Figure 10, where the blue symbols refer to Kennedy (1961), the green symbols to Guy et al. (1966) and the red symbols to Fukuoka et al. (1982). Circles indicate washed out dunes, diamonds upper plane bed, triangles are downstream migrating antidunes, squares denote upstream migrating antidunes, 'x' refers to standing waves, '-' chutes and pools and cyclic steps and 'T' bed configurations defined *transitional* by Guy et al. (1966).

Figure 10 clearly shows that the transition zones between lower and upper regime ($0.0003 < Q_s/Q_w < 0.0007$) and between upper regime bedforms migrating downstream and upper regime bedforms migrating upstream or the presence of a sheet flow layer ($0.0015 < Q_s/Q_w < 0.0032$) identified in Figure 9 well represent the equilibrium bed configuration observed by other researchers. Further, in agreement with Figure 9, points representing the standing waves are located in the transition zone with $0.0015 < Q_s/Q_w < 0.0032$. Finally, as indicated in Figure 9, points representing equilibrium cyclic steps and chute and pools are characterized by high values of Q_s/Q_w.

The non-dimensional plots of Figure 10 present the same changes in bedform geometry observed in the dataset of Figure 9. The non-dimensional parameter λ/H remains relatively constant and approximately equal to 3-5 for values of $Q_s/Q_w < 0.0015$ and it then increases rapidly as the equilibrium bed configuration transitions to standing waves, upstream migrating antidunes and cyclic steps (Figure 10 a). The gradual decrease in λ/D_g at the transition from washed out dunes to downstream migrating antidunes observed in Figure 9b is present in Figure 10b (the scale of the vertical axis in Figure 10b is logarithmic). As observed in Figure 9c for the experiments with fine sand, as Q_s/Q_w increases, the bedform height relative to the water depth Δ/H increases with heights of upstream migrating bedforms greater than 60% of the water depth (Figure 10c). Finally, Figure 10d confirms that significant suspended sand load was observed in experiments with upstream migrating bedforms (antidunes, chutes and pools and cyclic steps), downstream migrating antidunes formed with limited or negligible suspended load, and upper plane bed conditions occurred with and without suspended sand transport. Interestingly, at values of Q_s/Q_w typical of upstream migrating bedforms, the upper plane bed configurations seem to occur with values of u^*/v_s close to or smaller than 1, indicating limited suspended sand load.

6. Conclusions

Open channel flow experiments were conducted in a sediment feed flume to study the effect of sand supply rate and caliber on upper regime bedforms at equilibrium, that is when the flow conditions and the bed configuration do not change in time. The analysis of the results and the comparison with previous upper regime experiments suggest that 1) the ratio of the volume transport of sediment to the volume transport of water Q_s/Q_w plays a prime control on the equilibrium bed configuration, and 2) the presence of suspended sand load is critical for the formation of upstream migrating bedforms.

For values of Q_s/Q_w between 0.0003 and 0.0007, the bed configuration transitions from washed-out dunes (lower regime) to downstream migrating antidunes (upper regime). This transition is characterized by decreasing λ/D_g and constant values of λ/H. At values of Q_s/Q_w greater than 0.0015 the bedform wavelength increases and this corresponds to a change in bed configuration. This change in bed configuration depends on the sediment size. For values of Q_s/Q_w greater than 0.0032 upstream migrating antidunes and cyclic steps form in fine sand, while upper plane bed with bedload transport in sheet flow mode develops in coarse sand. Upper plane bed with a few grain diameters thick bedload layer was observed for a wide range of values of Q_s/Q_w. Standing waves seem to form for values of Q_s/Q_w when the downstream migrating antidunes evolve into a different bed configuration, that is when $0.0015 < Q_s/Q_w < 0.0032$.

Acknowledgments

The authors thank Gary Parker for translating relevant portions of the Fukuoka et al. (1982) paper. Sydney Sanders and Sadegh Jafarinik were supported with a grant from Exxon Mobil. Ryan Johnson, Amanda Balkus, Mahsa Ahmadpoor, Brandon Fryson and Briana McQueen were supported through the NSF award CBET 1751926 and the REU supplements.

Data Availability Statement

The dataset of all the experiments performed at the University of South Carolina are publicly available through the Dryad repository. The link to the experiments performed by Ricardo Hernandez Moreira, Sadegh Jafarinik and Sydney Sanders are https://doi.org/10.5061/dryad.c59zw3r9b, https://datadryad.org/stash/share/OUwXaqZ4eLIYcvSPyzKSd9pH0wU8vBwZhkpGa-wbAr8 and https://datadryad.org/stash/share/sC1Rt9LKtRcvTdS31KwsW4g1TU3MtrHban8mRfzlmf4 respectively. Hernandez Moreira experiments were made publicly available through the SEAD repository, which is not accessible anymore. Details on the experimental set up can be found at http://sedexp.net/experiment/setting-hydraulics-laboratory-limited-resources. The experiments by Sadegh Jafarinik will be made public as soon as the doi link is activated.

References

Alexander, J., Bridge, J. S., Cheel, R. J. & Leclair, S. F. (2001). Bedforms and associated sedimentary structures formed under supercritical water flows over aggrading sand beds. *Sedimentology*, 48, 133-152.

Araya, T. & Masuda, F. (2001). Sedimentary structures of antidunes: An overview. *Journal of the Sedimentological Society of Japan*, 53, 1-15.

Best, J. (2005). The fluid dynamics of river dunes: A review and some future research directions. *Journal of Geophysical Research*, 110 (F4), F04S02.

Best, J. L. & Brayshaw, A. C. (1985). Flow separation – a physical process for the concentration of heavy minerals within alluvial channels. *Journal of the Geological Society*, 142 (5), 747-755.

Best, J. & Bridge, J. (1992). The morphology and dynamics of low amplitude bedwaves upon upper stage plane beds and the preservation of planar laminae. *Sedimentology*, 39, 737-752.

Blom, A., Ribberink, J. S. & de Vriend, H. J. (2003). Vertical sorting in bed forms: Flume experiments with a natural and a trimodal sediment mixture. *Water Resources Research*, 39 (3), 1025.

Bourgeois, J. (1980). A transgressive shelf sequence exhibiting hummocky stratification: the Cape Sebastian sandstone (upper Cretaceous), Southwestern Oregon. *Journal of Sedimentary Petrology*, 50 (3), 681-702.

Bridge, J. S. & Best, J. L. (1988). Flow, sediment transport and bedform dynamics over the transition from dunes to upper-stage plane beds: implications for the formation of planar laminae. *Sedimentology*, 35, 753-763.

Brownlie, W. R. (1981). *Prediction of flow depth and sediment discharge in open channels*. Report No. KH-R-43A. W. M. Keck Laboratory of Hydraulics and Water Resources Division of Engineering and Applied Science, California Institute of Technology, Pasadena, California.

Carling, P. A. (2013). Freshwater megaflood sedimentation: What can we learn about generic processes? *Earth-Science Reviews*, 125, 87-113.

Carling, P. A. & Leclair, S. F. (2019). Alluvial stratification styles in a large, flash-flood influenced dryland river: The Luni River, That Desert, north-west India. *Sedimentology*, 66, 102-128.

Carling, P. A. & Shvidchenko, A. B. (2002). A consideration on the dune:antidune transition in fine gravel. *Sedimentology*, 49, 1269-1282.

Carling, P. A., Golz, E., Orr, H. G. & Radecki-Pawlik, A. (2000a). The morphodynamics of fluvial sand dunes in the River Rhine, near Mainz Germany. I. Sedimentology and morphology. *Sedimentology*, 47, 227-252.

559 Carling, P. A., Williams, J. J., Golz, E. & Kelsey, A. D. (2000b). The morphodynamics of fluvial sand
560 dunes in the River Rhine, near Mainz, Germany. II. Hydrodynamics and sediment transport.
561 *Sedimentology*, 47, 253-278.
562 Cartigny, M. J. B., Postma, G., van der Berg, J. H. & Mastbergen, D. R. (2011). A comparative study of
563 sediment waves and cyclic steps based on geometries, internal structure and numerical modeling.
564 *Marine Geology*, 280, 40-56.
565 Cartigny, M. J. B., Ventra, D., Postma, G. & van der Berg, J. H. (2014). Morphodynamics and sedimentary
566 structures of bedforms under supercritical-flow conditions: New insights from flume experiments.
567 *Sedimentology*, 61, 712-748.
568 Covault, J. A., Kostic, S., Paull, C. K., Sylvester, Z. & Fildani, A. (2017). Cyclic steps and related
569 supercritical bedforms: Building blocks of deep-water depositional systems, western North America.
570 *Marine Geology*, 393, 4-20.
571 Einstein, H. A. & Barbarossa, N. L. (1952). River channel roughness. *Transactions of the American Society*
572 *of Civil Engineers*, 117 (1), 1121–1146.
573 Endo, N., Masuda, F., Sakai, T. & Yokokawa, M. (2002). Grain fabric in cross laminated deposits
574 conformably superimposed on parallel laminae: Flume experiments and application to geologic
575 records. *Journal of the Geological Society of Japan*, 108 (7), 415-420.
576 Engelund, F. (1970). Instability of erodible beds. *Journal of Fluid Mechanics*, 42 (2), 225-244.
577 Engelund, F. & Fredsoe, J. (1982). Sediment ripples and dunes. *Annual review of Fluid Mechanics*, 14, 13-
578 37.
579 Engelund, F. & Hansen, E. (1967). *A monograph on sediment transport in alluvial streams*. Teknisk Forlag,
580 Copenhagen, Denmark.
581 Fedele, J. J. (2003). *Bedforms and gravity underflows in marine environments*. PhD Thesis, University of
582 Illinois at Urbana-Champaign.
583 Fedele, J. J., Hoyal, D., Barnaal, Z., Tulenko, J. & Awalt, S. (2016). Bedforms created by gravity flows. In
584 D. A. Budd, E. A. Hajek & S. J. Purkis (eds.) *Autogenic Dynamics and Self-Organization in*
585 *Sedimentary Systems*. SEPM Special Publication 106, 95-121.
586 Fredsoe, J. (1974). On the development of dunes in erodible channels. *Journal of Fluid Mechanics*, 64 (1),
587 1-16.
588 Froude, M. J., Alexander, J., Barclay, J. & Cole, P. (2017). Interpreting flash flood paleoflow parameters
589 from antidunes and gravel lenses: An example from Montserrat, West Indies. *Sedimentology*, 64, 1817-
590 1845.
591 Fukuoka, S., Okutsu, K. & Yamasaka, M. (1982). Dynamic and kinematic features of sand waves in upper
592 regime. *Proceeding of the Japan Society of Civil Engineering*, 323, pp. 77-89 (in Japanese).

Garcia, M. H. (2008). Sediment transport and morphodynamics. Chapter 2 in M. H. Garcia (ed.) *Sedimentation Engineering. Processes, Measurements, Modeling and Practice*, ASCE Manuals and Reports on Engineering Practice 110. ASCE, Reston, VA. pp. 21-163.

Hayashi, T. & Ozaki, S. (1979). Alluvial bedform analysis I: Formation of alternating bars and braids. Chapter 7 in H. W. Shen & H. Kikkawa (eds.) *Application of stochastic processes in sediment transport*. Water Resources Publications, Littleton, Colorado, USA.

Hernandez Moreira, R. R. (2016). *Deposits emplaced in upper regime*. PhD thesis, Univeristy of South Carolina at Columbia available at https://scholarcommons.sc.edu/.

Hernandez Moreira, R. R., Jafarinik, S., Sanders, S., Kendall, C. G. St. C., Parker, G. & Viparelli, E. (2020). Emplacement of massive deposits by sheet flow. *Sedimentology*, 67, 1951-1972.

Hiscott, R. N., Aksu, A. E., Flood, E. D., Kostylev, V. & Yasar, D. (2013). Widespread overspill from. Saline density-current channel and its interaction with topography on the south-west Black Sea shelf. *Sedimentology*, 60, 1639-1667.

Hughes Clarke, J. E., Short, A. N., Piper, D. J. W. & Mayer, L. A. (1990). Large-scale current-induced erosion and deposition in the path of the 1929 Grand Banks turbidity current. *Sedimentology*, 37, 613-629.

Ikeda, S. (1984). Prediction of alternate bar wavelength and height. *Journal of Hydraulic Engineering*, 110 (4), 371-386.

Jafarinik, S., Hernandez Moreira, R. & Viparelli, E. (2019). Alluvial morphodynamics of bedrock reaches transporting mixed-size sand. Laboratory experiments. *Journal of Geophysical Research: Earth Surface*, 124, 3067-3089.

Jerolmack, D. J. & Mohrig, D. (2005). Frozen dynamics of migrating bedforms. *Geology*, 33 (1), 57-60.

Kennedy, J. F. (1961). *Stationary waves and antidunes in alluvial channels*. Report KH-R-2 W. M. Keck Laboratory of Hydraulics and Water Resources Division of Engineering, California Institute of Technology, Pasadena, California.

Kleinhans, M. G. (2005). Grain-size sorting in grainflows at the lee side of deltas. *Sedimentology*, 52, 291-311.

Kostachuk, R., Best, J. & Villard, P. V. (2010). The influence of dunes on mixing in a migrating salt-wedge: Fraser River estuary, Canada. *Earth Surface Processes and Landforms*, 35, 460-465.

Kostic, S. (2014). Upper flow regime bedforms on levees and continental slopes: turbidity current flow dynamics in response to fine-grained sediment waves. *Geosphere*, 10 (6), 1094-1103.

Lang, J., Le Heron, D. P., van den Berg, J. H. & Winsemann, J. (2021). Bedforms and sedimentary structures related to supercritical flows in glacigenic settings. *Sedimentology*, 68, 1539-1579.

Latosinski, F. G., Amsler, M. L., Vionnet, C. A., Heredia Ligorria, A. I., Szupiany, R. N., Diaz Lozada, J. M., Garcia, C. M. & Garcia, M. H. (2022). The role of dunes in flow resistance in a large and a small river. The case of the Parana' and Tercero rivers, Argentina. *Journal of Hydraulic Research*, 60 (3), 389-407.

Myrow, P. M., Jerolmack, D. J. & Peron, J. T. (2018). Bedform disequilibrium. *Journal of Sedimentary Research*, 88, 1096-1113.

Naruse, H., Arai, K., Matsumoto, D., Takahashi, H., Yaashita, S., Tanaka, G. & Murayama, M. (2012). Sedimentary features observed in the tsunami deposits at Rikuzentakata City. *Sedimentary Geology*, 282, 199-215.

Nunez-Gonzalez, F. & Martin-Vide, J. P. (2010). Downstream-migrating antidunes in sand, gravel and sand-gravel mixtures. In A. Dittrich, K. Koll, J. Aberle & P. Geisenhainer (eds.) *Proceedings of the International Conference of Fluvial Hydraulics – River Flow 2010*. Karlsruhe: Bundesanstalt für Wasserbau, 393-400. ISBN 978-3-939230-00-7.

Ohata, K., Naruse, H. & Izumi, N. (2021). Linear stability analysis of plane beds under flows with suspended load. *Earth Surface Dynamics* Discussion Paper. https://doi.org/10.5194/esurf-2021-60

Ohata, K., Naruse, H., Yokokawa, M. & Viparelli, E. (2018). New bedform phase diagrams and discriminant functions for formative conditions of bedforms in open-channels. *Journal of Geophysical Research: Earth-Surface*, 122, 2139-2158.

Paola, C., Wiele, S. M. & Reinhart, M. A. (1989). Upper-regime parallel lamination as the result of turbulent sediment transport and low-amplitude bed forms. *Sedimentology*, 36, 47-59.

Parker, G. (2004). *1D sediment transport morphodynamics with applications to rivers and turbidity currents*. Copyrighted e-book available at http://hydrolab.illinois.edu/people/parkerg/.

Parkash, B. & Middleton, G. V. (1970). Downcurrent textural changes in Ordovician turbidite greywackes. *Sedimentology*, 14, 259-293.

Pen, S., Izumi, N. & Coutinho de Lima, A. (2018). Linear stability analysis of upper-regime bed waves including the effect of density stratification. *Journal of Japan Society of Civil Engineers*, Ser. B1 (Hydraulic Engineering), 74 (4), I_1099-I_1104.

Postma, G., Kleverlaan, K. & Cartigny, M. J. B. (2014). Recognition of cyclic steps in sandy and gravelly turbidite sequences, and consequences for the Bouma facies model. *Sedimentology*, 61, 2268-2290.

Sequeiros, O. E., Spinewine, B., Beaubouef, R. T., Sun, T., Garcia, M. H. & Parker, G. (2010). Bedload transport and bed resistance associated with density and turbidity currents. *Sedimentology*, 57, 1463-1490.

Simons, D. B. & Richardson, E. V. (1962). *Roughness on depth-discharge relations in alluvial channels*. Geological Survey Water-Supply Paper 1498-E. United States Government Printing Office, Washington D. C.

Simons, D. B. & Richardson, E. V. (1966). *Resistance to flow in alluvial channels*. Geological Survey Professional Paper 422-J. United States Government Printing Office, Washington D. C.

Slingerland, R. & Smith, N. D. (1986). Occurrence and formation of water-laid placers. *Annual Review of Earth and Planetary Sciences*, 14, 113-147.

Southard, J. B. & Boguchwal, L. A. (1990). Bed configurations in steady unidirectional water flows. Part 2. Synthesis of flume data. *Journal of Sedimentary Petrology* 60 (5), 658-679.

Spinewine, B., Sequeiros, O. E., Garcia, M. H., Beaubouef, R. T., Sun, T., Savoye, B. & Parker, G. (2009). Experiments on wedge-shaped deep sea sedimentary deposits in minibasins and/or on channel levees emplaced by turbidity currents. Part II. Morphodynamic evolution of the wedge and of the associated bedforms. *Journal of Sedimentary Research*, 79, 608-628.

Taki, K. & Parker, G. (2005). Transportational cyclic steps created by flow over an erodible bed. Part 1. Experiments. *Journal of Hydraulic Research*, 43 (5), 488-501.

Vanoni, V. A. (1974). Factors determining bed forms of alluvial streams. *Journal of the Hydraulics Division, Proceedings of the American Society of Civil Engineers*, 100 (HY3), 363-377.

van Rijn, L. (1984). Sediment transport, Part III: Bed Forms and alluvial roughness. *Journal of Hydraulic Engineering*, 110 (12), 1733-1754.

Viparelli, E., Solari, L. & Hill, K. M. (2015). Downstream lightening and upward heavying: Experiments with sediments differing in density. *Sedimentology*, 62, 1384-1407.

Wilson, K. C. (1987). Analysis of bed-load motion at high shear stress. *Journal of Hydraulic Engineering*, 113 (1), 97-103.

Wright, S. & Parker, G. (2004a). Density stratification effects in sand-bed rivers. *Journal of Hydraulic Engineering*, 130 (8), 783-795.

Wright, S. & Parker, G. (2004b). Flow resistance and suspended load in sand-bed rivers: simplified stratification model. *Journal of Hydraulic Engineering*, 130 (8), 796-805.

Yokokawa, M., Hasegawa, K., Kanbayashi, S. & Endo, N. (2010). Formative conditions and sedimentary structures of sandy 3D antidunes: an application of the gravel step-pool model to fine-grained sand in an experimental flume. *Earth Surface Processes and Landforms*, 35, 1720-1729.

Yokokawa, M., Takahashi, Y., Yamamura, H., Kishima, Y., Parker, G. & Izumi, N. (2011). Phase diagram for antidunes and cyclic steps based on suspension index, non-dimensional Chezy resistance coefficient and Froude number. In *Proceedings of the 7th IAHR Symposium on River, Coastal and Estuarine Morphodynamics* (RCEM 2011), 1789–1794.

Figure captions

Figure 1. Schematic representation of the laboratory flume. Drawing not to scale.

Figure 2. Grain size distributions of the sediment used in the experiments. Legend labels correspond to the sand geometric mean diameter D_g. Dashed lines are the grain size distributions representative of suspended sand load in the SS experiments.

Figure 3. Breaking and non-breaking upstream migrating antdunes in experiment a) 7-SS, b) 5-SS, c) 4-SS, d) 3-SS, e) 6B-SS, and f) 6B-SS.

Figure 4. Engelund phase diagram after Parker (2004) with the experiments of Table 2 (black marker line), of Hernandez Moreira (2016) and Hernandez Moreira et al. (2020) (grey marker line). Empty symbols indicate experiments with coarse sand ($D_g > 0.5$ mm) and symbols with grey fill are experiments with fine sand ($D_g \leq 0.5$ mm). Circles represent washed-out dunes, diamonds denote upper plane bed conditions with a few diameters thick bedload layer, triangles are downstream migrating antidunes and squares indicate upstream migrating antidunes. 'x' represents standing waves in experiment 2-SS (fine sand) and '+' indicates upper plane bed with bedload transport in sheet flow mode (coarse sand experiments).

Figure 5. Profiles of suspended sediment concentration measured during experiments 1-SS – 5-SS, 5-SJ, 6-SJ, 9-SJ and 10-SJ. z denotes an upward oriented vertical coordinate with origin on the channel bed, H the water depth and c the volumetric suspended sediment concentration. Line color indicates the sand geometric mean size and symbol color indicates the bed configuration. Grey, red, blue and black lines represent experiments with sand D_g equal to 0.62 mm, 0.43 mm, 0.34 mm and 0.22 mm, respectively. Green, black, red, blue and yellow symbols respectively denote bed configurations of washed-out dunes, downstream migrating antidunes, plane bed, standing waves and upstream migrating antidunes. The red-yellow symbol indicates a bed configuration at the transition between standing waves and upstream migrating antidunes (experiment 10-SJ).

Figure 6. Pictures of experiments with fine sand (D_g = 0.34 mm). As the mass feed rate G_s increases, bedform wavelength λ and height Δ increase.

Figure 7. Pictures of experiments with coarse sand (D_g = 0.62 mm). As the mass feed rate G_s increases, bedform wavelength λ increase and bedform height Δ decreases.

Figure 8. Pictures showing a change in equilibrium bed configuration with the water discharge.

Figure 9. Non-dimensional summary of the experiments presented in this paper and in Hernandez Moreira (2016) and Hernandez Moreira et al. (2020). H denotes the water depth, λ the bedform wavelength, D the characteristic sediment size, u^* the shear velocity and v_s the settling velocity of the sand geometric mean size D_g. Here, fine sand has $D_g \leq 0.5$ mm, and coarse sand has $D_g > 0.5$ mm. WD indicates washed out dunes, DA downstream migrating antidunes, UP upper plane bed with a few grain diameters thick bedload layer, SW standing waves, PS upper plane bed with bedload transport in sheet flow mode, UA upstream migrating antidunes. DA/WS and US/SW respectively denote bed configurations at the downstream migrating antidune – standing wave transition and at the upstream migrating antidune – standing wave transition. DA/PS refers to a bed configuration at the transition between downstream migrating antidunes and upper regime plane bed with bedload transport in sheet flow mode.

Figure 10. Data of experiments by Kennedy (1961) (blue symbols), Guy et al. (1966) (green symbols) and Fukuoka et al. (1982) (red symbols) in the non-dimensional plots of Figure 9. Circles denote dunes and washed out dunes, diamonds upper plane bed, triangles downstream migrating antidunes, 'x' standing waves, squares upstream migrating antidunes, '—' chutes and pools or cyclic steps, and 'T' in panel c indicate a bed configuration classified as transitional by Guy et al. (1966). Kennedy (1961) and Fukuoka et al. (1982) do not report measurements of bedform height.

Tables

Table 1. Summary of the experimental conditions. Experiments were run in two different experimental sets and are denoted by the lead experimentalist's initials (i.e. SS and SJ) along with each unique run number where experiment 1 ran by Sydney Sanders is denotated as 1-SS and experiment 3 ran by Sadegh Jafarinik is denoted 3-SJ. D_g denotes the geometric mean diameter of the sediment used in each experiment, Q_w is the flow discharge and G_s the mass sediment feed rate.

Run name	**D_g (mm)**	**Q_w (l/s)**	**G_s (kg/min)**
1-SJ	0.87	15	1.5
2-SJ	0.87	15	6
3-SJ	0.87	15	16
4-SJ	0.87	8	6
5-SJ	0.62	15	1
6-SJ	0.62	15	2.2
7-SJ	0.62	15	6.9
8-SJ	0.22	15	0.6
9-SJ	0.22	8	0.6
10-SJ	0.22	8	2.2
1-SS	0.43	30	10
2-SS	0.43	20	10
3-SS	0.43	10	10
4-SS	0.34	10	10
5-SS	0.34	10	15
6A-SS	0.34	10	20
6B-SS	0.34	5	20
7-SS	0.62	10	10

Table 2. Summary of the experimental results, where S = bed slope, H = flow depth, Fr_o = Froude number associated with skin friction, Δ = bedform height, λ= bedform wavelength, v = migration rate, negative values indicate upstream migrating bedforms. The bed configuration is reported using the following abbreviations: WD as washed-out dunes, UP as upper plane bed with a few grain diameters thick bedload layer, SW as standing waves, UA as upstream migrating antidunes, DA as downstream migrating antidunes, and PS as upper plane bed with bedload transport in sheet flow mode. The '--'indicates that bedform height or migration rate were not measured.

Run Name	S **(-)**	**H (cm)**	Fr_o **(-)**	**Δ (cm)**	**λ (cm)**	**v (cm/min)**	**Bed Configuration**
1-SJ	0.0057	8.70	0.98	1.8	33	35	WD
2-SJ	0.0110	6.16	1.65	1.5	30	60	DA
3-SJ	0.0211	5.32	2.05	0.5	45	18	PS
4-SJ	0.0178	3.97	1.43	--	65	--	UP
5-SJ	0.0049	10.27	0.76	2.8	38	30	WD
6-SJ	0.0074	7.91	0.90	3.2	25	29	DA
7-SJ	0.0135	4.87	2.35	--	35	--	UP
8-SJ	0.0024	10.17	0.85	0.8	10	17	WD
9-SJ	0.0029	8.42	0.83	1.0	10	18	WD
10-SJ	0.0049	6.36	1.08	1.8	28	17	UA/SW
1-SS	0.0072	13.14	1.06	--	0	--	UP
2-SS	0.0080	12.91	0.91	1.0	65	--	SW
3-SS	0.0150	3.96	2.13	2.0	50	-35	UA-breaking
4-SS	0.0140	4.09	2.03	3.0	50	-130	UA
5-SS	0.0130	4.98	1.18	4.5	80	-150	UA
6A-SS	0.0150	5.52	1.32	5.5	90	--	UA-breaking
6B-SS	0.0180	3.89	1.44	3.0	100	--	UA-breaking
7-SS	0.0110	5.92	1.07	1.0	55	-18	UA

Table 3. Comparison between bedform height Δ, wavelength λ and bed configuration in experiments performed with coarse sand with D_g = 0.87 mm (SJ) and D_g = 1.11 mm (RHM). Q_w denotes the flow discharge and G_s the mass feed rate. The bed configuration is reported using the following abbreviations: WD as washed-out dunes, DA as downstream migrating antidunes, and PS as upper plane bed with bedload transport in sheet flow mode.

Run Name	**Q_w (l/s)**	**G_s (kg/min)**	**Δ (cm)**	**λ (cm)**	**Bed Configuration**
1-SJ	15	1.5	1.8	33	WD
RHM	20	1.5	3.8	78	WD
RHM	30	1.5	4.0	77	WD
2-SJ	15	6	1.5	30	DA
RHM	30	6	5.0	42	DA
3-SJ	15	16	0.5	45	PS
RHM	20	16	1.0	70	PS
RHM	30	16	4.0	80	PS

Figures

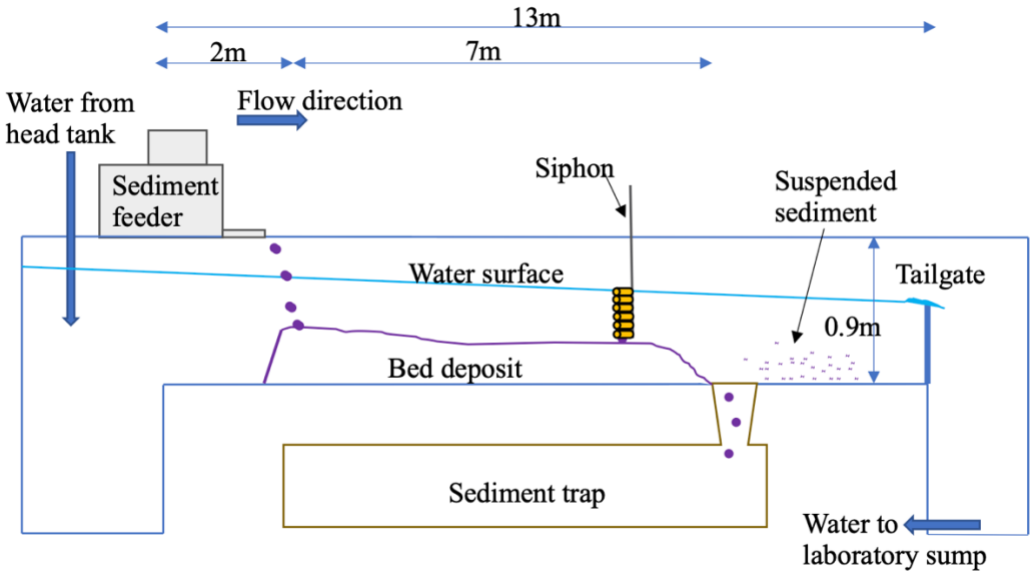

Figure 1. Schematic representation of the laboratory flume. Drawing not to scale.

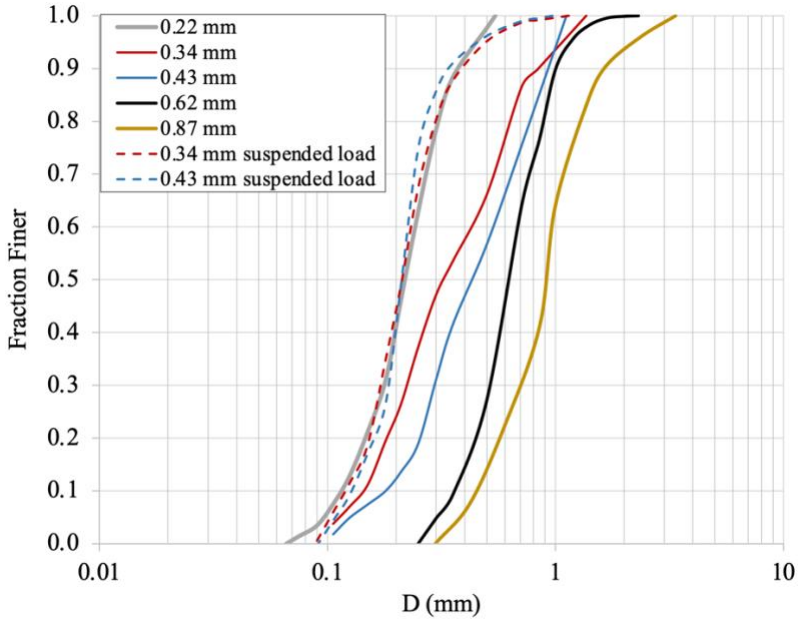

Figure 2. Grain size distributions of the sediment used in the experiments. Legend labels correspond to the sand geometric mean diameter D_g. Dashed lines are the grain size distributions representative of suspended sand load in the SS experiments.

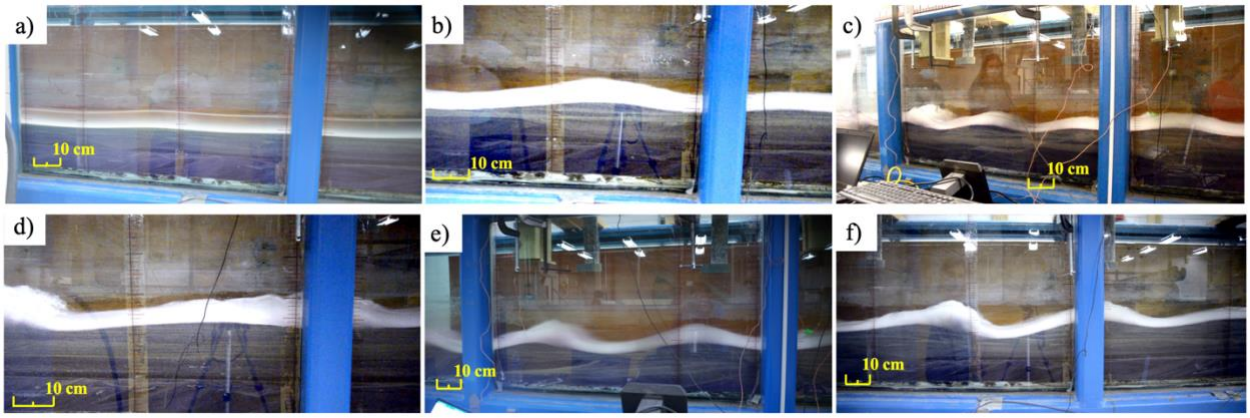

Figure 3. Breaking and non-breaking upstream migrating antdunes in experiment a) 7-SS, b) 5-SS, c) 4-SS, d) 3-SS, e) 6B-SS, and f) 6B-SS.

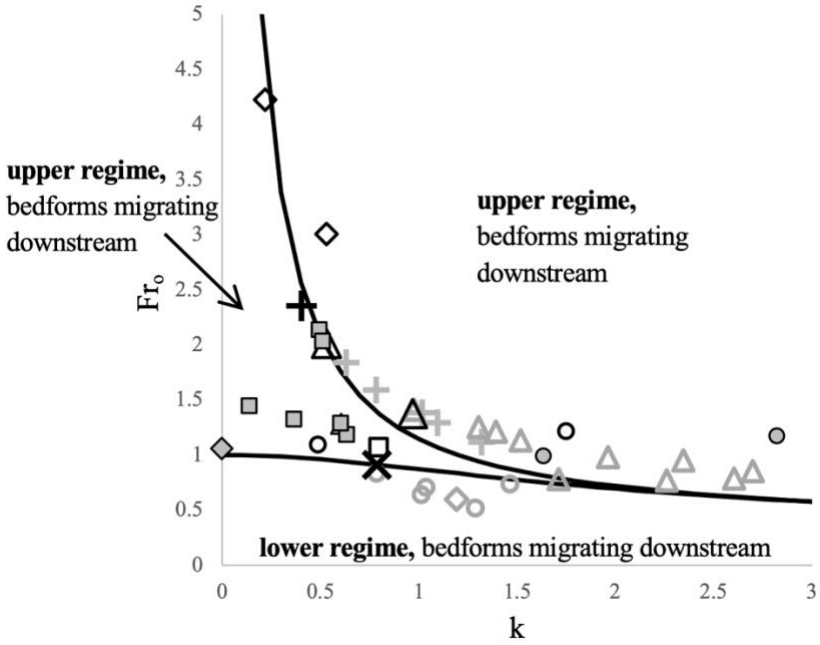

Figure 4. Engelund phase diagram after Parker (2004) with the experiments of Table 2 (black marker line), of Hernandez Moreira (2016) and Hernandez Moreira et al. (2020) (grey marker line). Empty symbols indicate experiments with coarse sand (D_g > 0.5 mm) and symbols with grey fill are experiments with fine sand ($D_g \leq 0.5$ mm). Circles represent washed-out dunes, diamonds denote upper plane bed conditions with a few diameters thick bedload layer, triangles are downstream migrating antidunes and squares indicate upstream migrating antidunes. 'x' represents standing waves in experiment 2-SS (fine sand) and '+' indicates upper plane bed with bedload transport in sheet flow mode (coarse sand experiments).

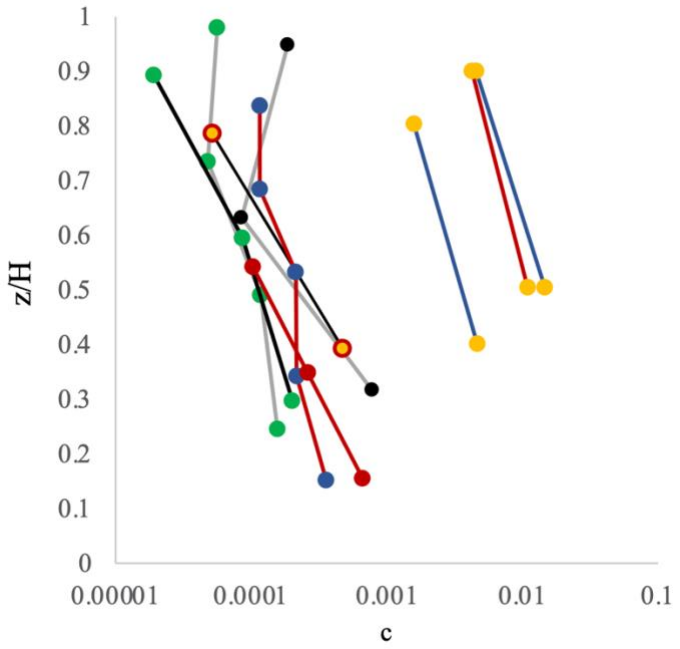

Figure 5. Profiles of suspended sediment concentration measured during experiments 1-SS – 5-SS, 5-SJ, 6-SJ, 9-SJ and 10-SJ. *z* denotes an upward oriented vertical coordinate with origin on the channel bed, *H* the water depth and *c* the volumetric suspended sediment concentration Line color indicates the sand geometric mean size and symbol color indicates the bed configuration. Grey, red, blue and black lines represent experiments with sand D_g equal to 0.62 mm, 0.43 mm, 0.34 mm and 0.22 mm, respectively. Green, black, red, blue and yellow symbols respectively denote bed configurations of washed-out dunes, downstream migrating antidunes, plane bed, standing waves and upstream migrating antidunes. The red-yellow symbol indicates a bed configuration at the transition between standing waves and upstream migrating antidunes (experiment 10-SJ).

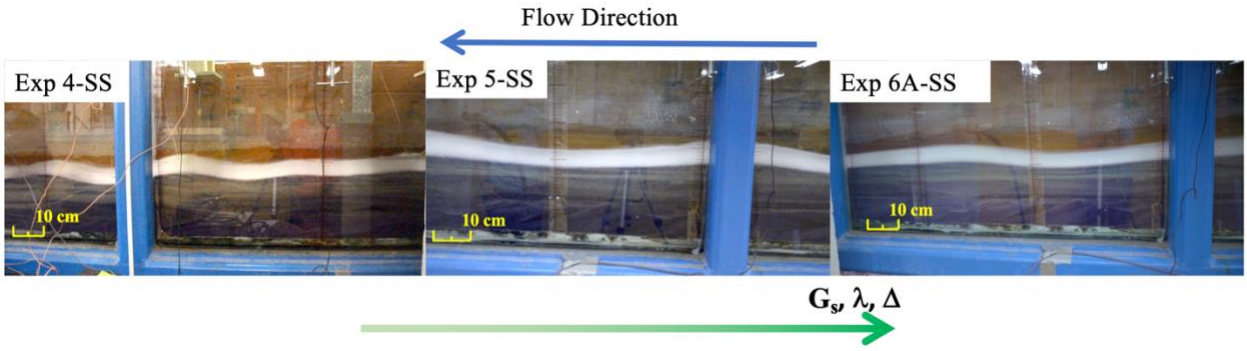

820

821 **Figure 6.** Pictures of experiments with fine sand (D_g = 0.34 mm). As the mass feed rate G_s increases,
822 bedform wavelength λ and height Δ increase.

823

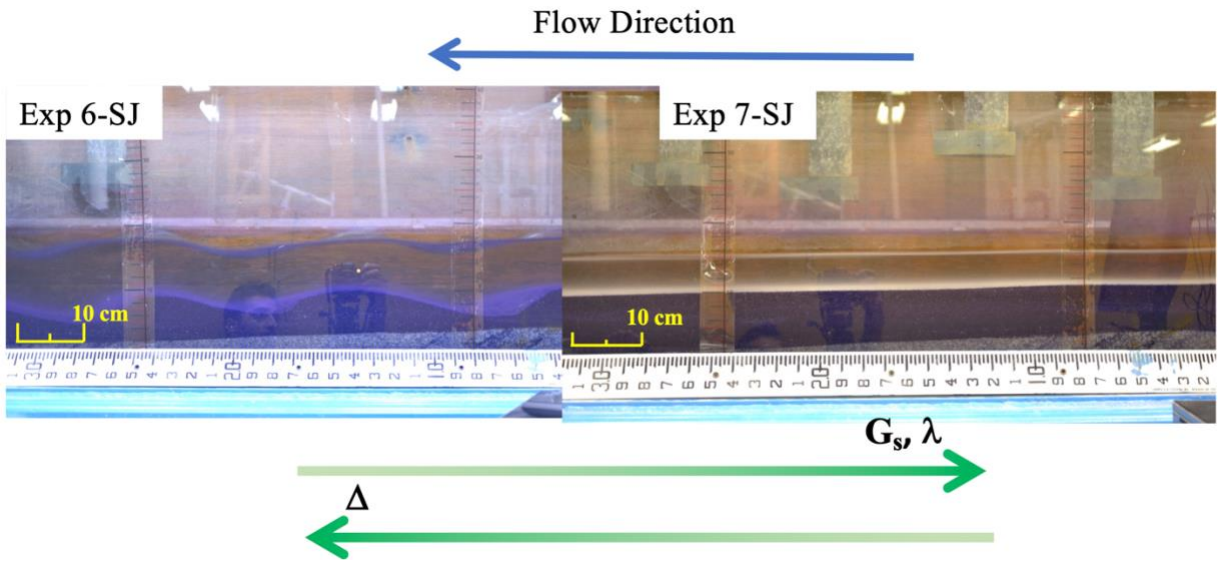

824

825 **Figure 7.** Pictures of experiments with coarse sand (D_g = 0.62 mm). As the mass feed rate G_s increases,
826 bedform wavelength λ increase and bedform height Δ decreases.

827

828

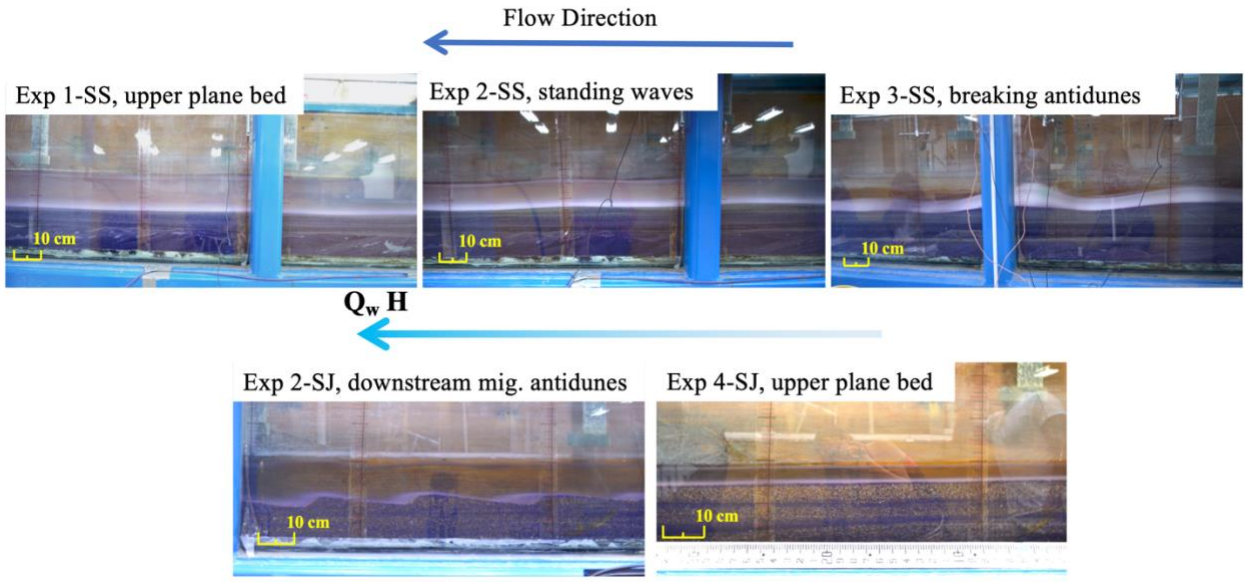

Figure 8. Pictures showing a change in equilibrium bed configuration with the water discharge Q_w and the flow depth H.

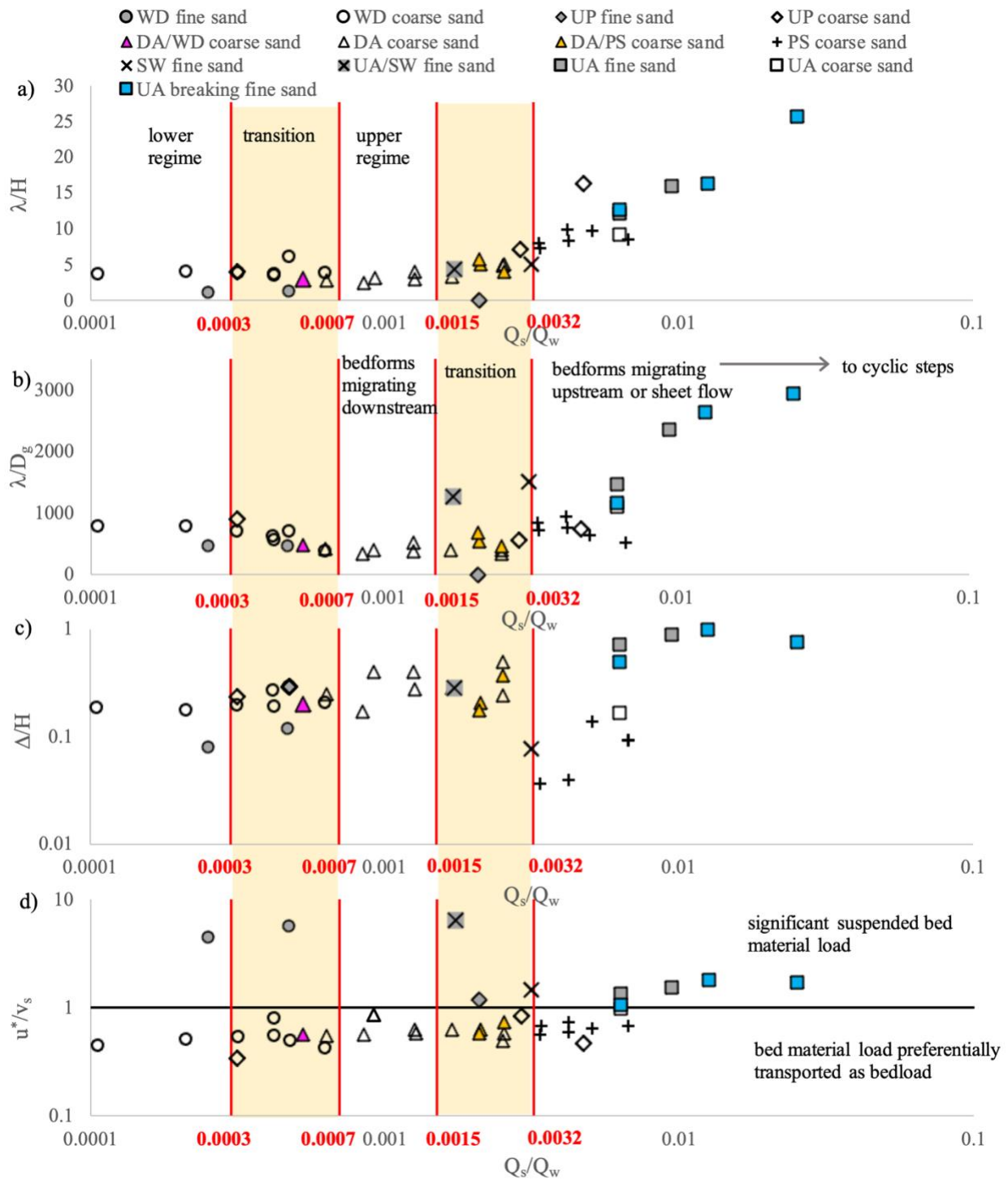

Figure 9. Non-dimensional summary of the experiments presented in this paper and in Hernandez Moreira (2016) and Hernandez Moreira et al. (2020). H denotes the water depth, λ the bedform wavelength, D the characteristic sediment size, Δ the bedform height, u^* the shear velocity and v_s the settling velocity of the sand geometric mean size D_g. Here, fine sand has $D_g \leq 0.5$ mm, and coarse sand has $D_g > 0.5$ mm. WD indicates washed out dunes, DA downstream migrating antidunes, UP upper plane bed with a few grain

840 diameters thick bedload layer, SW standing waves, PS upper plane bed with bedload transport in sheet flow
841 mode, UA upstream migrating antidunes. DA/WS and US/SW respectively denote bed configurations at
842 the downstream migrating antidune – standing wave transition and at the upstream migrating antidune –
843 standing wave transition. DA/PS refers to a bed configuration at the transition between downstream
844 migrating antidunes and upper regime plane bed with bedload transport in sheet flow mode.
845
846
847

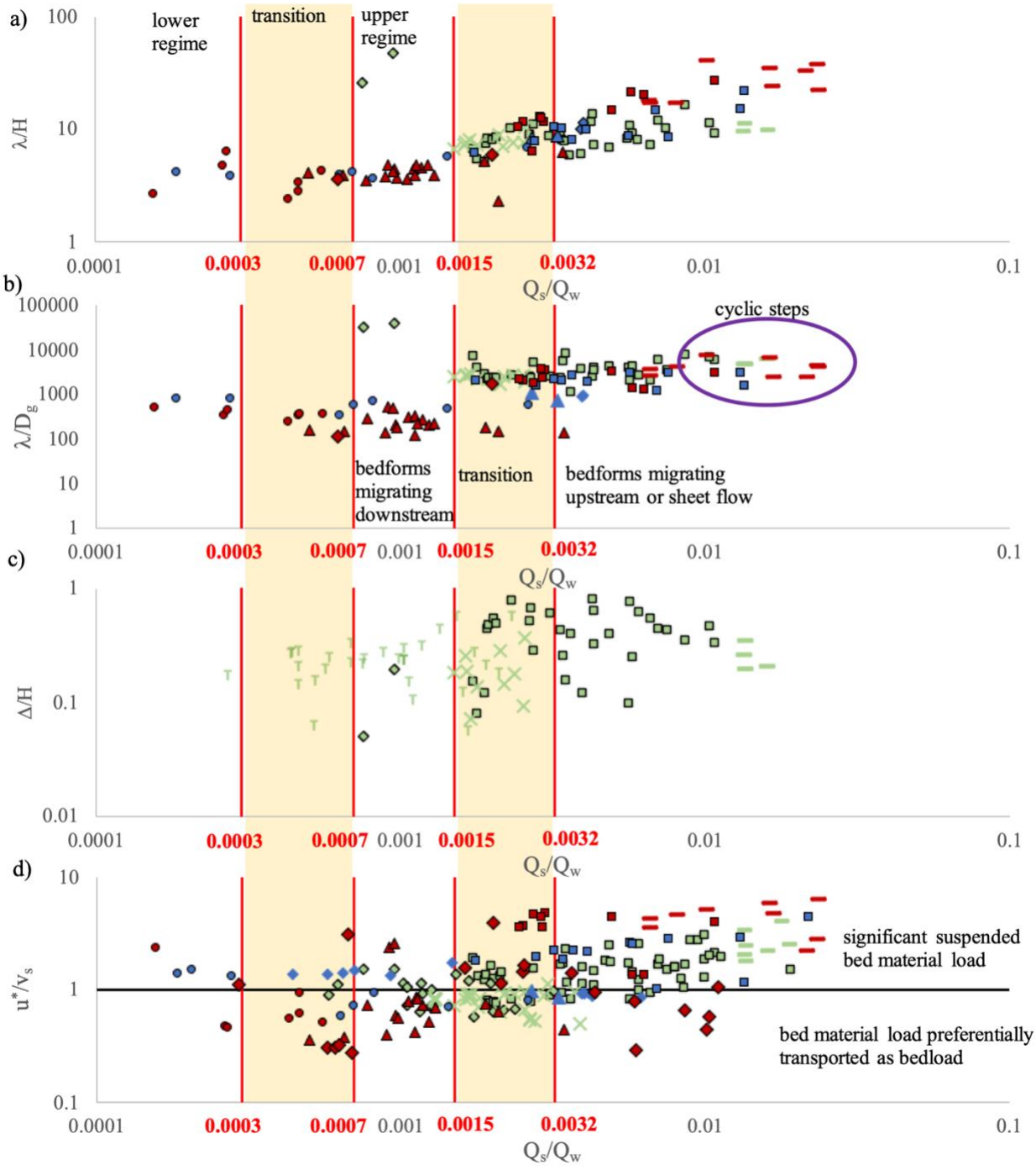

Figure 10. Data of experiments by Kennedy (1961) (blue symbols), Guy et al. (1966) (green symbols) and Fukuoka et al. (1982) (red symbols) in the non-dimensional plots of Figure 9. Circles denote dunes and washed out dunes, diamonds upper plane bed, triangles downstream migrating antidunes, 'x' standing waves, squares upstream migrating antidunes, '—' chutes and pools or cyclic steps, and 'T' in panel c indicate a bed configuration classified as transitional by Guy et al. (1966). Kennedy (1961) and Fukuoka et al. (1982) do not report measurements of bedform height.